Structural properties and quasiparticle energies of cubic SrO, MgO and $SrTiO_3$

2000 J. Phys.: Condens. Matter 12 3671

(http://iopscience.iop.org/0953-8984/12/15/315)

J. Phys.: Condens. Matter **12** (2000) 3671–3688. Printed in the UK PII: S0953-8984(00)10731-3

Structural properties and quasiparticle energies of cubic SrO, MgO and $SrTiO_3$

Giancarlo Cappellini†, Sophie Bouette-Russo‡, Bernard Amadon‡, Claudine Noguera‡ and Fabio Finocchi‡

† INFM Sezione di Cagliari and Dipartimento di Fisica, Università di Cagliari, Cittadella Universitaria, Strada Provinciale Monserrato—Sestu km 0.700, I-09042 Monserrato (Ca), Italy
‡ Laboratoire de Physique des Solides, UMR CNRS 8502, Bâtiment 510, Université Paris-Sud, 91405 Orsay, France

Received 4 January 2000

Abstract. The structural properties and the band structures of the charge-transfer insulating oxides SrO, MgO and $SrTiO_3$ are computed both within density functional theory in the local density approximation (LDA) and in Hedin's GW-scheme for self-energy corrections, by using a model dielectric function, which approximately includes local field and dynamical effects. The deep valence states are shifted by the GW-method to higher binding energies, in very good agreement with photoemission spectra. Since in all of these oxides the direct gaps at high-symmetry points of the Brillouin zone may be very sensitive to the actual value of the lattice parameter a already at the LDA level, self-energy corrections are computed both at the theoretical and the experimental a. For MgO and SrO, the values of the energies of transition between the valence and the conduction bands are improved by GW-corrections, while for $SrTiO_3$ they are overestimated. The results are discussed in relation to the importance of local field effects and to the nature of the electronic states in these insulating oxides.

1. Introduction

In addition to forming the major constituent of the outer crust of the earth, oxides are of considerable interest for their wide applications in various technological fields such as electrochemistry, catalysis and microelectronics [1]. They present very diverse electronic ground states which range from superconducting, metallic and semiconducting (intrinsic, charge-density-like or spin-density-like) to insulating. From a theoretical point of view, a proper description of their electronic properties is still an area of active research. On the one hand, several transition metal oxides require the inclusion of many-body effects beyond the available effective one-electron approaches, such as the density functional theory (DFT) or the *ab initio* Hartree–Fock (HF) method. On the other hand, even for insulating charge-transfer oxides, such as MgO and SrO, whose electronic ground states are well accounted for in a one-electron picture, the calculation of quasiparticle (QP) energies within the DFT or the HF method gives rather poor results. Indeed, one has to face the so-called energy band-gap problem [2]. Indeed, when using the Kohn–Sham eigenvalues of the highest occupied and the lowest empty states, the resulting gap usually underestimates the experimental data. On the other hand, the corresponding difference between the HF eigenvalues overestimates the gap severely. Alternative ways to calculate the band gap in infinite systems have been found, in the framework of HF or DFT. One of them is based on total-energy differences between

0953-8984/00/153671+18$30.00

ground and charge-transfer states [3]. The other one relies on the value of the gap found in the one-electron spectrum of the ionized or hole-doped system [4]. However, such methods are unable to provide the full QP spectrum.

In the last decade, due to the implementation of angle-resolved photoemission experiments able to cope with charging effects on insulating oxides, detailed QP spectra of MgO [5], $SrTiO_3$ [6] and TiO_2 [7, 8], among other oxides, have become available. The experimental achievements demand systematic improvements in the theoretical description of the electronic excitations of simple oxides.

In semiconducting and ionic crystalline compounds, corrections to the DFT eigenvalues, as obtained from the Kohn–Sham equations, may be estimated by first-order many-body perturbation theory [9–11], with respect to the difference between the exchange–correlation (XC) self-energy and the corresponding XC potential of the DFT, for which various approximations are available. Within the same approach, the self-energy operator is treated in the GW-approximation proposed by Hedin [9]. Such calculations have been carried out with success for several semiconducting and insulating crystals [10–15], permitting the prediction of the quasiparticle energies and the calculation of optical properties of real solids.

One of the crucial points in such calculations is the evaluation of the self-energy operator, which is numerically very expensive, because of the requirement of knowledge of the full inverse dielectric matrix of the system under study. This is a bottleneck in the application of the method to systems with large number of atoms in the unit cell, such as surfaces [16, 17] and defect-containing or low-symmetry solids. In order to reduce the substantial numerical burden and to be able to predict electronic excited states for a wider range of real systems, one may use efficient GW-methods, in which a model dielectric function is used to mimic the screening properties of the system under study.

Pioneering work in this direction has been performed by Bechstedt and Del Sole in a tight-binding scheme [18] and by Gygi and Baldereschi [19] within the DFT in the local density approximation (LDA) for the exchange and correlation energy. The key to their work relies (i) on the use of a model dielectric function, which mimics the main screening properties of semiconductors, and (ii) on an approximated self-energy operator in which both local fields and dynamical screening—giving rise to opposite contributions to band gaps—are neglected [10, 18, 19]. For a large family of semiconductors, the band gaps obtained through these simplified methods show good accordance with both experiments and full GW-results, in which the screening properties of the system are calculated from first principles. More recently, an efficient GW-method that approximately includes dynamical screening and local field effects, without increasing the computational effort required, has been formulated [20] and proved to reproduce quasiparticle energies and band gaps for bulk zinc-blende solids (ranging from Si, GaAs and AlAs to the more ionic ZnSe) [21] and non-cubic systems (BN [22], SiC polytypes [23, 24]) satisfactorily. The method is based on a linear expansion of the dynamical contribution to the exchange–correlation self-energy, on the use of a model dielectric function and on a local *ansatz* for the treatment of the intrinsically non-local screened interaction. Depending on the system, the calculation may be speeded up by two orders of magnitude with respect to the corresponding full GW-calculations. Moreover, this kind of GW-calculation is feasible on a standard workstation.

The aim of the present paper is to study the ground-state properties of cubic magnesium oxide, strontium oxide and strontium titanate, in the DFT-LDA scheme, as well as their quasiparticle band structures within the efficient GW-scheme. On one hand, no previous GW-calculation of SrO or $SrTiO_3$ exists, to our knowledge. On the other hand, these charge-transfer oxides are characterized by different fundamental gaps, ranging from $\simeq$3 eV ($SrTiO_3$) to $\simeq$7.7 eV (MgO), as given by experimental data. Their band structures may substantially

differ from those of the semiconductors cited above, due to the presence of strongly localized electronic states. Thus, such a study may also represent a test for the approximate GW-scheme, originally proposed for small-gap semiconductors, as regards its capabilities for a different class of physical system.

The paper is organized as follows. The theoretical framework is described in section 2 and this is followed, in section 3, by a description of the computational ingredients used for the description of structural and electronic properties of MgO, SrO and $SrTiO_3$. The results obtained for these systems are presented separately in sections 4, 5 and 6, respectively. Finally, in section 7 we present our conclusions and the perspectives opened up by our work.

2. GW-corrections

The energy $E_{n\vec{k}}$ of a quasiparticle in a band n at a given $\vec{k}$-point in the Brillouin zone can be obtained through the equation [10, 11, 25]

$$\left[-\frac{\nabla^2}{2} + V_{\rm ext}(\vec{r}) + V_{\rm H}(\vec{r})\right]\phi_{n\vec{k}}(\vec{r}) + \int {\rm d}^3\vec{r}'\ \Sigma(\vec{r},\vec{r}';E_{n\vec{k}})\phi_{n\vec{k}}(\vec{r}') = E_{n\vec{k}}\phi_{n\vec{k}}(\vec{r}) \tag{1}$$

which is written in atomic units ($e = \hbar = m_e = 1$). $V_{\rm ext}(\vec{r})$ is the external potential originating from the ions, $V_{\rm H}(\vec{r})$ is the Hartree potential and Σ is the mass operator, usually called the self-energy operator, which is in general non-local, non-Hermitian and energy dependent. In principle it contains the exchange and correlation effects and is state ($n\vec{k}$) dependent. One can compare the above equation to that of Kohn and Sham [26]:

$$\left[-\frac{\nabla^2}{2} + V_{\rm ext}(\vec{r}) + V_{\rm H}(\vec{r}) + V_{\rm xc}(\vec{r})\right]\psi_{n\vec{k}}(\vec{r}) = E^{(0)}_{n\vec{k}}\psi_{n\vec{k}}(\vec{r}) \tag{2}$$

where $V_{\rm xc}$ is the exchange–correlation potential of the DFT (for which several approximation are available), and the superscript (0) will denote the quantities computed at the DFT level from now on. $E^{(0)}_{n\vec{k}}$ is usually considered as a first approximation to the quasiparticle energy. The failure of this scheme for evaluating energies of transition $E_{n'\vec{k}} - E_{n\vec{k}}$ between different quasiparticle states in solids has been evidenced by many authors [2, 10, 11].

One can correct the DFT eigenvalues $E^{(0)}_{n\vec{k}}$ in a first-order perturbation theory with respect to $\Sigma_{n\vec{k}} - V_{\rm xc}$, and estimate the QP energies as

$$E_{n\vec{k}} \simeq E^{(0)}_{n\vec{k}} + \langle\psi_{n\vec{k}}|\Sigma(\vec{r},\vec{r}';E_{n\vec{k}}) - V_{\rm xc}(\vec{r})|\psi_{n\vec{k}}\rangle. \tag{3}$$

The evaluation of $\Sigma(r, r'; E_{n\vec{k}})$ is in general a very difficult task. A possible approach is to use the GW-approximation [9] in which a perturbation expansion for the self-energy can be constructed and stopped at the first order:

$$\Sigma(\vec{r},\vec{r}';\omega) = {\rm i}\int_{-\infty}^{+\infty}\frac{{\rm d}\omega'}{2\pi}\,{\rm e}^{+{\rm i}\delta\omega'}G(\vec{r},\vec{r}';\omega+\omega')W(\vec{r},\vec{r}';\omega') \tag{4}$$

where G is the one-particle Green function, W is the screened Coulomb interaction and $\delta = 0^+$. Following Bechstedt and co-workers [2, 20], the real part of the self-energy operator (which is relevant for the corrections to the QP band structure) may be separated into a dynamic and a static contribution, and written as

$$\Re\,\Sigma(\vec{r},\vec{r}';\omega) = \Sigma^{\rm sex}(\vec{r},\vec{r}') + \Sigma^{\rm coh}(\vec{r},\vec{r}') + \Sigma^{\rm dyn}(\vec{r},\vec{r}';\omega). \tag{5}$$

$\Sigma^{\rm sex}$ and $\Sigma^{\rm coh}$ are the static screened exchange (SEX) and the Coulomb-hole (COH) terms, respectively, and $\Sigma^{\rm dyn}$ the energy-dependent contribution. Although the previous equation is purely formal, it is the starting point of simplified GW-schemes, since one can work out approximated expressions for each contribution separately. The most expensive step towards

the evaluation of GW-corrections to $E^{(0)}_{n\vec{k}}$ is the calculation of the energy-dependent screened interaction $W(r, r'; \omega)$. Although many improvements have been proposed for an efficient calculation of the dielectric response function from first principles [27, 28], this stage is still very demanding as regards both computer time and memory when a large basis set is used for the description of the electronic structure. In particular, this is the case for oxides in a plane-wave pseudopotential approach. On the other hand, the improvement of DFT-LDA band structures obtained by using schemes originally formulated on a phenomenological basis, such as those based on the scissor operator or Slater's α-potential [2], showed that the essential physics can be described through the use of effective or state-dependent potentials. From a more fundamental point of view, one can work out a model for the screening properties of the system, and see to what extent the computed QP spectra account for the observed experimental values. Possibly, the model should also be simple enough to be generalized to a large number of different systems. Following previous studies [20, 23], we use a model dielectric function to estimate both the static and the dynamical contributions to the self-energy (equation (5)), since it is the key ingredient in efficient GW-approximations.

2.1. Static screening and local field effects

For the diagonal part of the screening function, we use an analytical model originally proposed by Bechstedt and Del Sole [18]:

$$\epsilon(q, \bar{\rho}) = 1 + \left[\frac{1}{\epsilon_\infty - 1} + \frac{q^2}{q_{TF}^2} + \frac{3q^4}{4k_F^2 q_{TF}^2} \right]^{-1} \tag{6}$$

where the Fermi vector k_F and the Thomas–Fermi wave-vector q_{TF} depend on the average electron density $\bar{\rho}$. This expression mimics the free-electron-gas behaviour at high q. At $q = 0$, equation (6) gives the value of the optical dielectric constant ϵ_∞ of the oxide. Moreover we use a local *ansatz* for the static Coulomb screened interaction, analogously to that of Hybertsen and Louie [27]:

$$W(\vec{r}, \vec{r'}) = \frac{1}{2}[W^h(\vec{r} - \vec{r}'; \rho(\vec{r})) + W^h(\vec{r} - \vec{r}'; \rho(\vec{r}'))] \tag{7}$$

where W^h is the screened Coulomb interaction of a virtual homogeneous system characterized by a finite optical dielectric constant [18, 29]. Quasiparticle energies determined from the above *ansatz* result in good accordance with full GW-calculated ones [20, 27]. This, together with equation (6), permits us to obtain a simple analytical expression for the static part of the Coulomb-hole self-energy Σ^{coh}. The explicit formula has been given elsewhere [30]. For the calculation of Σ^{sex} in equation (5), the Fourier transform of $W(\vec{r}, \vec{r}')$ is needed, namely $\tilde{W}(\vec{k} + \vec{G}, \vec{k} + \vec{G}')$. In order to reduce sharply the time needed to compute this term, we proceed in two steps. Firstly, we retain only the diagonal terms in the screened Coulomb interaction. Secondly, we account for local field effects (i.e. non-diagonal terms with $\vec{G} \neq \vec{G}'$ in $\tilde{W}$) by using suitable state-dependent densities to compute k_F and q_{TF}. Given a state $n\vec{k}$, we define the effective electron density $\tilde{\rho}_{n\vec{k}}$, which determines the typical screening lengths q_{TF}^{-1} and k_F^{-1} relevant for the estimation of $E_{n,\vec{k}}$ (equation (3)) as the expectation value of the ground-state electronic density $\rho(\vec{r})$ for the actual state:

$$\tilde{\rho}_{n\vec{k}} = \int \mathrm{d}^3\vec{r}\ \rho(\vec{r}) |\psi_{n\vec{k}}(\vec{r})|^2. \tag{8}$$

Since the relevant screening lengths k_F^{-1} and q_{TF}^{-1} are increasing functions of $\tilde{\rho}_{n\vec{k}}$, the latter is intended to give an approximate description of the local fields in Σ^{sex} through an enhanced screening for the electronic states which contribute effectively to the total electron density.

In the oxides considered here, the effective densities $\tilde{\rho}_{n\vec{k}}$ range from few tenths of the mean valence electron density $\bar{\rho} = Z_{\rm val}/V$ for conduction states up to 4–5 $\bar{\rho}$ for deep valence states. As a consequence, the lengths k_F^{-1} and q_{TF}^{-1} are shorter for the screening of valence band states than for that of conduction band states. This difference is enhanced with respect to that for more covalent semiconductors, such as Si and GaAs [20], in which the valence electron distribution is more delocalized and less dissimilar to that of the conduction states than for oxides such as MgO.

This approximate scheme for treating local field effects was analysed in detail and its reliability was shown through a comparison with full GW-calculations, in the case of both small- and wide-gap semiconductors [20,21]. In reference [21], it was also shown that the use of a non-diagonal model dielectric function does not clearly improve band gaps while adding additional computational costs.

2.2. Dynamical contributions

The diagonal matrix element of the dynamical part of the self-energy (the third operator on the right-hand side in equation (5)) for the state $\psi_{n\vec{k}}$:

$$\Sigma^{\rm dyn}_{n\vec{k}}(\omega) = \langle \psi_{n\vec{k}} | \Sigma^{\rm dyn}(\vec{r}, \vec{r}'; \omega) | \psi_{n\vec{k}} \rangle \tag{9}$$

can be linearly expanded in energy around the DFT value $E^{(0)}_{n\vec{k}}$, with the linear coefficient

$$\beta_{n\vec{k}} = \langle \psi_{n\vec{k}} | \left(\frac{\partial \Sigma}{\partial \omega} \right)_{E^{(0)}_{n\vec{k}}} | \psi_{n\vec{k}} \rangle. \tag{10}$$

This approximation for the energy dependence of the self-energy operator turns out to be valid over a wide energy range, as confirmed by the results of full GW-calculations on bulk Si [10]. Solving the Dyson equation within the first-order perturbation theory with respect to $\Sigma - V_{\rm xc}$, and using equations (3) and (5), the QP shifts for the $\psi_{n\vec{k}}$ state hence read

$$E_{n\vec{k}} - E^{(0)}_{n\vec{k}} = \frac{\Sigma^{\rm coh}_{n\vec{k}} + \Sigma^{\rm sex}_{n\vec{k}} + \Sigma^{\rm dyn}_{n\vec{k}}(E^{(0)}_{n\vec{k}}) - \langle \psi_{n\vec{k}} | V_{\rm xc} | \psi_{n\vec{k}} \rangle}{1 + \beta_{n\vec{k}}} \tag{11}$$

where $\Sigma^{\rm coh}_{n\vec{k}}$ and $\Sigma^{\rm sex}_{n\vec{k}}$ are the expectation values of the static COH and SEX contributions to the self-energy, respectively. From the GW-expression for Σ, replacing G by $G^{(0)}$, computed at the DFT level [20]:

$$\Sigma^{\rm dyn}_{n\vec{k}}(E^{(0)}_{n\vec{k}}) = \sum_{n'\vec{k}'} \int \frac{{\rm d}^3\vec{q}}{(2\pi)^3} |B^{\vec{k}\vec{k}'}_{nn'}(\vec{q})|^2 \frac{4\pi}{q^2} (E^{(0)}_{n\vec{k}} - E^{(0)}_{n'\vec{k}'}) \times P \int_0^\infty \frac{{\rm d}\omega}{\omega\pi} \frac{\Im\left(\epsilon^{-1}(\vec{q}, \tilde{\rho}_{n\vec{k}}, \omega)\right)}{\omega - {\rm sgn}(E^{(0)}_{n'\vec{k}'} - \mu)(E^{(0)}_{n\vec{k}} - E^{(0)}_{n'\vec{k}'})} \tag{12}$$

$$\beta_{n\vec{k}} = \sum_{n'\vec{k}'} \int \frac{{\rm d}^3\vec{q}}{(2\pi)^3} |B^{\vec{k}\vec{k}'}_{nn'}(\vec{q})|^2 \frac{4\pi}{q^2} P \int_0^\infty \frac{{\rm d}\omega}{\pi} \frac{\Im\left(\epsilon^{-1}(\vec{q}, \tilde{\rho}_{n\vec{k}}, \omega)\right)}{\left[\omega - {\rm sgn}(E^{(0)}_{n'\vec{k}'} - \mu)(E^{(0)}_{n\vec{k}} - E^{(0)}_{n'\vec{k}'})\right]^2} \tag{13}$$

where

$$B^{\vec{k}\vec{k}'}_{nn'}(\vec{q}) = \int {\rm d}^3\vec{r}\ \psi^*_{n\vec{k}}(\vec{r}) {\rm e}^{{\rm i}\vec{q}\cdot\vec{r}} \psi_{n'\vec{k}'}(\vec{r}). \tag{14}$$

The model ϵ^{-1} is diagonal in q-space and the local field effects are accounted for through the use of the state averaged density $\tilde{\rho}_{n\vec{k}}$ (equation (8)). The ω-dependent dielectric function is

obtained from the static one by means of the plasmon-pole approximation (PPA) [10]. The PPA has been widely used to compute semiconductor and insulator quasiparticle band structures, even in the energy range of semicore states [12–14]. In order to account for the differences $E^{(0)}_{n\vec{k}} - E^{(0)}_{n'\vec{k}'}$ in equations (12) and (13), replacing them with the state-independent form

$$E^{(0)}_{n\vec{k}} - E^{(0)}_{n'\vec{k}'} \approx -q^2/2$$

as in reference [20], and using the sum rule $\sum_{n'\vec{k}'} |B^{\vec{k}\vec{k}'}_{nn'}(\vec{q})|^2 = 1$, one obtains

$$\Sigma^{\mathrm{dyn}}_{n\vec{k}}(E^{(0)}_{n\vec{k}}) \simeq \int \frac{\mathrm{d}^3\vec{q}}{(2\pi)^3}\, P \int_0^\infty \frac{\mathrm{d}\omega}{\omega\pi}\, \frac{\Im\left(\epsilon^{-1}(\vec{q}, \tilde{\rho}_{n\vec{k}}, \omega)\right)}{\omega + q^2/2} \tag{15}$$

$$\beta_{n\vec{k}} \simeq \int \frac{\mathrm{d}^3\vec{q}}{(2\pi)^3}\, \frac{4\pi e^2}{q^2} P \int_0^\infty \frac{\mathrm{d}\omega}{\pi}\, \frac{\Im\left(\epsilon^{-1}(\vec{q}, \tilde{\rho}_{n\vec{k}}, \omega)\right)}{(\omega + q^2/2)^2}. \tag{16}$$

Therefore, once the spectrum and eigenfunctions obtained in the framework of the DFT are known, the calculation of $\Sigma^{dyn}_{n\vec{k}}(E^{(0)}_{n\vec{k}})$ and $\beta_{n\vec{k}}$ according to equations (15) and (16) needs no additional external parameters apart from the model dielectric function, and this is a simple task that can be carried out on a standard workstation.

We have made extensive checks to test the reliability of the approximations used to obtain equations (15) and (16), in the case of silicon. Some transitions between high-symmetry points of some valence and conduction band states in Si are compared in table 1 to those obtained through full GW-approximation. The energy of the transitions between high-symmetry points, as well as the fundamental gap in Si, are in very close agreement with those obtained from full GW-calculations and with experiments for both methods. As far as the QP eigenvalues in Si are concerned, the top of the valence band $\Gamma_{25',v}$ is shifted downwards with respect to the DFT values of 0.28 eV. This can be compared with the upward shift of 0.07 eV, as found by Godby *et al* [11].

Table 1. Computed vertical transitions and minimal valence–conduction band gaps for silicon (in eV). The experimental values are quoted in reference [27].

Si	Full GW[a]	Full GW[b]	This work	Experiment
$\Gamma_{1,v}$–$\Gamma_{25',v}$	12.04		12.09	12.5 ± 0.6
$\Gamma_{25',v}$–$\Gamma_{15,c}$	3.35	3.30	3.33	3.4
$\Gamma_{25',v}$–$\Gamma_{2',c}$	4.08	4.27	4.25	4.2
$L_{2',v}$–$\Gamma_{25',v}$	9.79		9.98	9.3 ± 0.4
$L_{1,v}$–$\Gamma_{25',v}$	7.18		7.27	6.7 ± 0.2
$L_{3',v}$–$\Gamma_{25',v}$	1.27		1.25	1.2 ± 0.2, 1.5
$\Gamma_{25',v}$–$L_{1,c}$	2.27	2.30	2.22	2.4 ± 0.2, 2.1
$\Gamma_{25',v}$–$L_{3,c}$	4.24	4.11	4.15	4.15 ± 0.1
$L_{3',v}$–$L_{1,c}$	3.54		3.47	3.45
$L_{3',v}$–$L_{3,c}$	5.51		5.41	5.50
$X_{4,v}$–$\Gamma_{25',v}$	2.99		2.98	3.3 ± 0.2, 2.9
$\Gamma_{25',v}$–$X_{1,c}$	1.44		1.54	1.3
Valence–conduction minimal gap	1.29	1.24	1.21	1.17

[a] Reference [27].
[b] Reference [11].

3. Computational details

The density functional calculations are carried out within the LDA for exchange and correlation [31]. The Kohn–Sham orbitals are expanded in a plane-wave basis set. Special care has been taken in constructing the pseudopotentials for cations (Sr, Ti, Mg), in order to avoid the occurrence of ghost states [32] and to ensure an optimal transferability over a wide energy range. We find that the inclusion of semicore states, such as 4s and 4p states for Sr, and 3s and 3p states for Ti, greatly improves the transferability of the pseudopotentials, and is at the same time necessary to take into account the hybridization of cation semicore states with O 2s states.

Angular components up to $l = 2$ are included. The scheme of Martins and Troullier is used [33] to generate separable soft norm-conserving pseudopotentials, with core radii (in Bohr) of: 2.00 (Sr, 4s), 1.50 (Sr, 4p), 1.90 (Sr, 4d); 1.30 (Ti, 3s), 1.40 (Ti, 3p), 1.80 (Ti, 3d); 1.38 (O, 2s), 1.60 (O, 2p), 1.38 (O, 3d); 2.00 (Mg, 3s, 3p, 3d). The cut-off energy needed to obtain a convergence better than 0.1 eV of both total energy and Kohn–Sham eigenvalues is found to be equal to 50 Ryd for MgO, 60 Ryd for SrO and 80 Ryd for $SrTiO_3$.

The use of ten special $\vec{k}$-points [34] for charge integration in the irreducible wedge of the Brillouin zone (IBZ) is sufficient to achieve a good accuracy for the computed total energy; for instance, the total energy changes by less than 10 meV and the fundamental band gap by less than 0.1 eV when using ten instead of six special points to sample the IBZ.

The main bottleneck in the *ab initio* GW-calculations is the calculation and the inversion of the full dielectric matrix for the eigenfunctions and eigenvalues of the system. Typically, this task takes approximatively 75% of the CPU time needed for the calculation of the self-energy correction for a single state [2]. As a result of the use of a model screening, the computational cost and memory requirement are strongly reduced, and are comparable to those of calculations carried out within the DFT. Efficient GW-calculations can thus be carried out also on a standard workstation†.

The evaluation of the GW-corrections to the LDA band structures, and especially of the SEX contribution Σ^{sex} to the self-energy, needs some care, due to the presence of an integrable divergence. A reduction of the numerical effort by using a limited number of k-points in the IBZ is possible through the method proposed by Gygi and Baldereschi [35]. In our calculations, the regularization is performed, for all the $\vec{k}$-points for which Σ^{sex} is calculated, by transforming the integral over the BZ of the diverging contribution into an integral of a function $F(\vec{k})$ (periodic over the BZ), that can be computed analytically, plus a discrete sum over special $\vec{k}$-points of a smooth function. For the sake of conciseness, in the case of the bare exchange term (the generalization to the case of the diagonal screened exchange in cubic systems is straightforward), the transformation reads

$$\Omega \int_{\mathrm{BZ}} \frac{\mathrm{d}^3k'}{(2\pi)^3} \frac{|B_{nn'}^{\vec{k}\vec{k}'}(\vec{g})|^2}{|\vec{k}' - \vec{k} - \vec{g}|^2} \simeq \Omega \int_{\mathrm{BZ}} \frac{\mathrm{d}^3k'}{(2\pi)^3} F(\vec{k}')|B_{nn'}^{\vec{k}\vec{k}'}(0)|^2 + \sum_{\vec{k}'} w_{\vec{k}'} \left[\frac{|B_{nn'}^{\vec{k}\vec{k}'}(\vec{g})|^2}{|\vec{k}' - \vec{k} - \vec{g}|^2} - \theta^{\mathrm{BZ}}(\vec{k}' - \vec{k} - \vec{g})|B_{nn'}^{\vec{k}\vec{k}'}(0)|^2 F(\vec{k}' - \vec{k}) \right]. \tag{17}$$

$\theta^{\mathrm{BZ}}(\vec{q}) = 1$ if $\vec{q} \in$ BZ and zero otherwise, $B_{nn'}^{\vec{k}\vec{k}'}(\vec{g})$ has previously been defined (equation (14)) and $w_{\vec{k}}$ is the weight associated with the special point $\vec{k}$ in the IBZ. By following this method, ten special $\vec{k}$-points in the IBZ are sufficient to get a converged Σ^{sex} within few tens of meV.

† We used both a Cray C90 computer and a Digital α-500 workstation, with 512 MB of memory.

Because of the presence of the static screened exchange term, each GW-correction to a given $E^{(0)}_{n\vec{k}'}$ scales as $N_{\vec{k}}NN_{\mathrm{PW}}$, where $N_{\vec{k}}$, N and N_{PW} are the numbers of $\vec{k}$-points used in the summation of the charge, of occupied electronic states and of the plane waves used in the expansion of the Kohn–Sham orbitals, respectively.

4. Magnesium oxide

The ground-state properties obtained for the O_h^5 phase (rock-salt) of magnesium oxide are summarized in table 2. They are computed by fitting the curve of the total energy versus the lattice parameter to the equation of state proposed by Murnaghan. One can note that our results compare well to other all-electron LDA calculations [15, 36] and show slight discrepancies with respect to experimental data: the computed lattice parameter is underestimated by about 2% and the cohesive energy is about 15% too large. We attribute these errors mainly to the use of the LDA.

Table 2. Structural properties of cubic MgO. A comparison is made with other LDA calculations, in a pseudopotential approach [41] or using LMTO [15, 36].

MgO	a (Å)	B (Mbar)	E_{coh} (eV)
Experiment	4.211	1.55 [40]	10.33
Reference [41]	4.191	1.46	
Reference [15]	4.16		
Reference [36]	4.09	1.71	10.67
Present work	4.125	1.56	11.80

The band structures, both in the LDA and including quasiparticle corrections, are shown in figure 1 along high-symmetry lines in the BZ. In the following, we refer to the energy levels relative to the top of the valence band in the LDA calculation, which is arbitrarily set to zero. The bands are calculated at the theoretical equilibrium lattice parameter $a_{\mathrm{th}} = 4.125$ Å. In table 3 we detail the energy differences between electronic states at high-symmetry points in the BZ, computed either at the theoretical equilibrium lattice parameter $a_{\mathrm{th}} = 4.125$ Å or at the experimental one $a_{\mathrm{exp}} = 4.211$ Å. One can easily see that some of the direct transitions, and in particular those at Γ, strongly depend upon the value of the lattice parameter. This is true at the LDA level, while the GW-corrections are less sensitive to the actual value of a. In ionic rock-salt compounds, the value of the fundamental gap at the Γ point is indeed driven by the strong Madelung potential, which varies as the inverse of the lattice parameter.

In agreement with a previous full GW-calculation [15], the quasiparticle corrections consist of a rigid shift of the conduction band (CB) with respect to the valence band (VB)—that is, application of a scissor operator, which is modulated by smooth $\vec{k}$-dependent terms of the order of 10% of the rigid shift itself. The total valence bandwidth, $\Gamma_{15,v}$–$\Gamma_{1,v}$, changes from 17.3 eV in the LDA to 20.1 eV with quasiparticle corrections. Similarly, the L′ and X_1 points move $\simeq$2 eV downwards from the valence band maximum (VBM), as one can see from figure 1. This improves the accordance with the experimental XPS spectra which show a main peak at 18 eV and a shoulder at 21 eV below the VBM [37]. The fundamental band gap moves from 5.21 eV to 8.88 eV.

In all these calculations, we assume the experimental value $\epsilon_\infty = 2.95$ [38] for the static dielectric constant. Recently, through an *ab initio* calculation of the dielectric function within the LDA, Shirley found $\epsilon_\infty = 3.03$, at the experimental lattice parameter [39]. In order to test the sensitivity of our theoretical scheme to the choice of ϵ_∞, which enters as a parameter in our

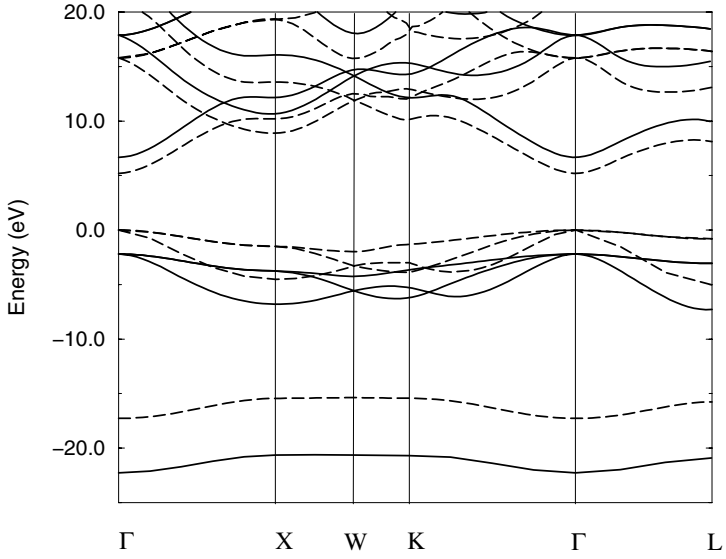

Figure 1. Computed bands of cubic MgO at the theoretical lattice parameter. Solid lines: GW-bands. Dashed lines: LDA bands. The top of the LDA valence bands is arbitrarily set to zero.

Table 3. Direct gaps of cubic MgO (in eV). Our results are given both in the LDA and with quasiparticle corrections (LDA + GW), either at the theoretical equilibrium lattice constant (†) or at the experimental one (‡). The theoretical calculations of references [15, 39, 43] were all carried out at the experimental lattice constant.

MgO	$E_g(\Gamma)$	$E_g(X)$	$E_g(L)$	Minimal gap
Experiment [42]	7.7	13.3	10.8	7.7 (Γ–Γ)
HF + polarization [43]	8.21	15.79	11.48	8.21 (Γ–Γ)
LDA [15]	5.2	10.5	8.9	5.2 (Γ–Γ)
LDA + GW [15]	7.7	13	11.4	7.7 (Γ–Γ)
LDA [39]	4.73			4.73 (Γ–Γ)
LDA + GW [39]	7.81			7.81 (Γ–Γ)
This work				
LDA†	5.21	10.40	8.93	5.21 (Γ–Γ)
LDA‡	4.61	10.26	8.46	4.61 (Γ–Γ)
LDA + GW†	8.88	14.43	12.99	8.88 (Γ–Γ)
LDA + GW‡	8.20	14.22	12.46	8.20 (Γ–Γ)

model screening function defined in equation (6), we performed an additional GW-calculation by adopting $\epsilon_\infty = 3.50$. Consistently with a stronger screening, the direct transition energies at high-symmetry points are lowered by $\simeq$0.5 eV at most.

It is interesting to note that the main corrections to the Kohn–Sham eigenvalues of VB states come from the static screened exchange term Σ^{sex} (equation (8)), while the Coulomb-hole contribution Σ^{coh} dominates the quasiparticle corrections to the eigenvalues of the CB. For instance, $\Sigma^{sex}_{\Gamma_1} \simeq -16$ eV and $\Sigma^{coh}_{\Gamma_1} \simeq -10$ eV at the bottom of the VB, while $\Sigma^{sex}_{\Gamma_1} \simeq -5$ eV and $\Sigma^{coh}_{\Gamma_1} \simeq -8$ eV at the bottom of the CB. This is consistent with the more localized nature of the VB states with respect to the CB states. The same remark applies to SrO and $SrTiO_3$,

which are discussed in the following sections.

As far as the interpretation of the main optical transitions is concerned, we indicate in table 3 the experimental values with their tentative assignment, according to Schömberger and Aryasetiawan [15]. We agree with their interpretation, since our GW-values, computed at the experimental lattice constant, differ by $\simeq$1 eV at most from theirs. Our calculations slightly overestimate the experimental transition energies.

5. Strontium oxide

The ground-state properties computed for the O_h^5 phase of SrO are summarized in table 4. The band structures, computed in the LDA and with QP corrections, along high-symmetry directions are shown in figure 2.

Table 4. Structural properties of cubic SrO. A comparison is made with Hartree–Fock [48] and LDA calculations [36, 49].

SrO	a (Å)	B (Mbar)	E_{coh} (eV)
Experiment	5.16	0.906	10.45
HF [48]	5.25	1.06	
LDA [49]	5.1–5.18	0.88–0.82	10.9–10.5
LDA [36]	5.22	1.07	9.59
Present work	5.07	1.04	11.9

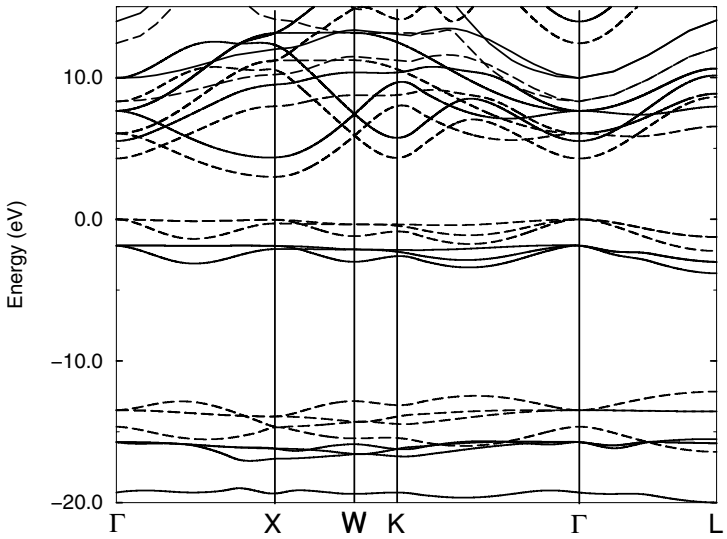

Figure 2. Computed bands of cubic SrO, at the theoretical lattice parameter. Dashed lines: LDA bands. Full lines: GW-bands. The zero is arbitrarily fixed at the top of the valence LDA band.

A deep band, originating mainly from Sr 4s states, is not shown in the figure. It is found at around −30.5 eV in the LDA calculation, with a dispersion less than 1 eV. The QP corrections shift this band to lower energies, about 33 eV below the valence band maximum (VBM).

The bands of lowest energy shown in figure 2 originate from Sr 4p and O 2s states. In the LDA, the bandwidth is about 4.3 eV, while the GW-corrections push that band towards higher

binding energies, and split it into two less dispersive structures, of which the lower originates from O 2s states mainly, and the upper from Sr 4p states. The splitting between O 2s and Sr 4p levels is essentially due to the larger Σ^{sex} contribution for the former states, as a consequence of their stronger localization.

As far as the deep VB levels are concerned, XPS experiments [37] found two broad peaks at $\simeq -35$ eV (A) and $\simeq -17.5$ eV (B) below the top of the valence band. The authors assigned the A structure to the band arising from Sr 4s states, and the B structure to those coming from O 2s and Sr 4p states. The resolution, however, was too poor for them to resolve the two latter contributions to peak B. The positions of the deep VB levels are badly accounted for in the LDA, which would yield the A peak at -30.5 eV and a broader B structure at around -13 eV. On the other hand, Hartree–Fock calculations including correlation [43] give a separation of about 6.5 eV between the O 2s and the Sr 4p states, which is probably overestimated. A better agreement with experimental data is obtained through the inclusion of GW-corrections, which shift the Sr 4s band to $\simeq -33$ eV and give two contributions to the electronic density of states at $\simeq -18$ eV and $\simeq -14$ eV with respect to the VBM, about 0.5 eV wide. The latter seem consistent with the broad B structure seen in XPS [37]. A later XPS investigation [44] found a splitting Δ_{AB} between the A and the B structure equal to 17.9 eV, which was interpreted as the difference in binding energy of the Sr 4s and 4p levels in SrO. Since it seems difficult to disentangle the Sr 4p and the O 2s contribution to the B structure, we compare the minimum and the maximum splittings Δ_{AB} as obtained in our calculations. In the LDA, Δ_{AB} ranges from 14.5 eV to 17.5 eV, while that obtained by including the GW-corrections ranges from 16 eV to 19 eV and agrees better with the XPS data.

The upper part of the valence band is very similar in the LDA and GW-calculations. Its width is 2.2 eV in the LDA and 2.1 eV after GW-corrections. The dispersions of both QP and LDA eigenvalues along high-symmetry directions are very similar, too.

The lower part of the conduction band drawn in the figures is shifted upward by GW-corrections, opening the LDA gap by about 3 eV, with additional and small corrections depending on the particular band and $\vec{k}$-point as one can see in table 5. In particular, the direct gap at Γ (X) passes from $E_g(\Gamma) = 4.29$ eV ($E_g(\text{X}) = 3.03$ eV) in LDA to $E_g(\Gamma) = 7.54$ eV ($E_g(\text{X}) = 6.39$ eV) after GW-corrections. It is important to note that the Γ_{15}–Γ_1 direct gap is very sensitive to the precise value of the lattice parameter a_0: while the above value $E_g(\Gamma) = 4.29$ eV is calculated at the LDA equilibrium lattice parameter a_{th}, at $a_{\text{exp}} = 5.16$ Å

Table 5. The gap of cubic SrO (in eV), at the high-symmetry point of the Brillouin zone. The gaps are calculated either at the theoretical lattice parameter (†) or at the experimental one (‡).

SrO	$E_g(\Gamma)$	E_g(X)	E_g(L)	Minimal gap
Experiment				
Reference [45]	5.896	6.28		5.9 (Γ–Γ)
Reference [46]	6.08	5.79		
LDA (reference [36])	4.26			3.8 (Γ–X)
X_α (reference [47])	5.10	4.03	7.3	3.9 (Γ–X)
HF + correction (reference [43])	7.11	9.11	12.36	8.54 (Γ–Γ)
Present work				
LDA†	4.29	3.03	7.79	3.00 (Γ–X)
LDA‡	3.92	3.11	7.47	3.04 (Γ–X)
LDA + GW†	7.54	6.39	11.17	6.37 (Γ–X)
LDA + GW‡	7.12	6.45	10.81	6.39 (Γ–X)

we find a smaller $E_g(\Gamma) = 3.92$ eV, i.e. a reduction of about 0.4 eV. The behaviour at the X point is different, since the $E_g(X)$ calculated at a_{exp} is equal to 3.11 eV, about 0.1 eV bigger than that computed at a_{th}. Given the different natures of the electronic states at the various symmetry points in the BZ, a non-trivial dependence of the eigenvalues upon the structural parameters is generally expected†.

On the other hand, the QP energy differences obtained by our method are less dependent on the precise value of the optical dielectric constant used in the model screening (equation (6)). For instance, $E_g(\Gamma)$ varies only by -3% when passing from $\epsilon_\infty = 3.35$ to $\epsilon_\infty = 3.7$, which represents an 11% increase of the optical dielectric constant.

We are not aware of any angle-resolved photoemission or inverse photoemission experiments on SrO, able to provide direct experimental information on the band dispersion around the Fermi level. Thus, the comparison of our results to experimental data is mainly based on the information issuing from reflectivity measurements. Rao and Kearney [45] conclude, for direct gaps at Γ (X), $E_g(\Gamma) = 5.9$ eV ($E_g(X) = 6.28$ eV), and exciton binding energies at high-symmetry points of the BZ around 0.2–0.3 eV. Conversely, more recent optical measurements on well characterized single crystals of SrO [46] found $E_g(X) = 5.79$ eV, lower than $E_g(\Gamma) = 6.08$ eV. On the basis of the onset of the optical absorption spectra, the authors also deduce that SrO has an indirect minimum gap, while BaO shows a direct gap at X. On the theoretical side, the nature of the fundamental gap of SrO is still debated: while both LMTO/LDA [36] and APW X_α [47] calculations give a Γ_{15}–X_3 indirect gap that is clearly underestimated (3.8 and 3.9 eV respectively), Pandey and co-workers [43] found more realistic values, $E_g(\Gamma) = 7.11$ eV and $E_g(X) = 9.11$ eV, through a Hartree–Fock calculation including correlation at the second order in perturbation theory. These results confirm the general findings on other semiconducting and insulating materials, that DFT-LDA underestimates the fundamental gap, while the reverse happens in Hartree–Fock calculations, although the inclusion of correlations in the latter improves the agreement with experiments. Our GW-corrected bands at the experimental lattice parameter yield gaps at X and Γ equal to $E_g(X) = 6.45$ eV and $E_g(\Gamma) = 7.12$ eV respectively, presenting a better agreement with experimental data.

6. Strontium titanate

The computed ground-state properties of the cubic phase of $SrTiO_3$, such as the equilibrium lattice parameter, the bulk modulus and the cohesive energy, are shown in table 6. A good agreement with previous LDA calculations [50, 51] is found. We stress that in all these calculations the self-consistent electron density includes the semicore states (Sr 4s, Sr 4p, Ti 3s and Ti 3p). With respect to experimental data, a slight underestimate (-1.3%) of the lattice parameter is obtained, while the computed cohesive energy is $\simeq$20% larger than that measured, as is usual in the LDA. As far as the GW-calculation is concerned, we adopt the experimental value $\epsilon_\infty = 5.82$ of the optical dielectric constant of the cubic phase of $SrTiO_3$ [52]. Both LDA and GW-bands (figure 3) are computed at the LDA theoretical equilibrium lattice parameter a_{th}.

Firstly, we discuss the positions of the deep-lying states not shown in figure 3. A deep, almost non-dispersive, energy band is found at $\simeq -54$ eV below the top of the valence band (VBM) in the LDA calculations, which originates from Ti 3s states. The inclusion of QP corrections in our GW-scheme pushes it downward, to -58.9 eV below the VBM. This is in very good agreement with XPS measurements [37], which show a peak at around -59 eV.

† In SrO, the bottom of the conduction band $X_{3,c}$ has mainly Sr 4d character, while at $\Gamma_{1,c}$ the Sr 5s character prevails. In any case, a noticeable degree of second-neighbour hybridization is present.

Table 6. Structural properties of cubic $SrTiO_3$. References [50,51] both use the LDA with ultrasoft pseudopotentials. The experimental values of a and E_{coh} are quoted in reference [56] and B is taken from reference [57].

$SrTiO_3$	a (Å)	B (Mbar)	E_{coh} (eV)
Experiment	3.903	1.83	31.7
Reference [50]	3.870	1.94	
Reference [51]	3.864	1.99	
This work	3.850	2.03	37.88

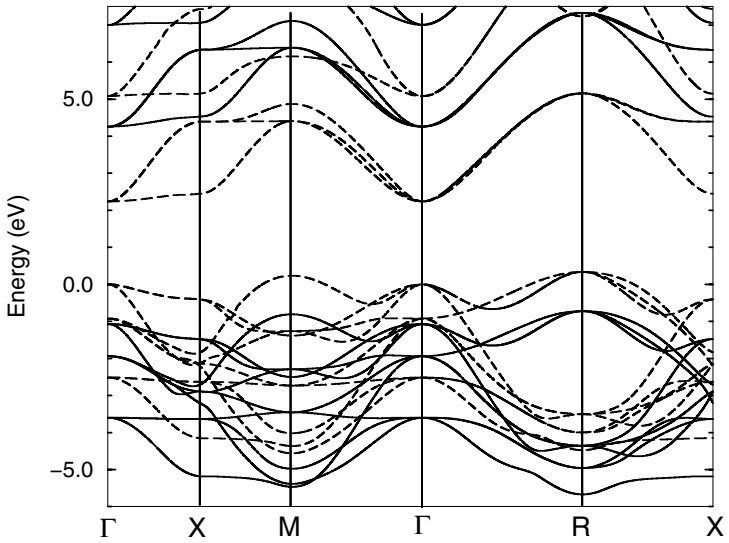

Figure 3. The upper part of the valence bands and lower part of the conduction bands of cubic $SrTiO_3$, at the theoretical equilibrium lattice parameter. Dashed lines: LDA bands. Solid lines: GW-bands.

Analogously, in the LDA calculation, the narrow bands originating mainly from Ti 3p states are located at −30.5 eV below the VBM, very close to a band with dominant Sr 4s character, at about −29.5 eV. GW-corrections push them to −33.7 eV and −32.7 eV, respectively. The XPS spectra show an asymmetric peak 2 eV wide, centred at $\simeq$−34.5 eV [37]. As found for the Ti 3s band, the inclusion of quasiparticle effects greatly improves the agreement with the experimental data.

The very broad structure in the XPS data [37] between −20 eV and −14 eV originating from O 2s and Sr 4p states is fully consistent with the position of our GW-bands, while the LDA bands are higher in energy by about 3 eV on average.

The valence band portion shown in figure 3 has a dominant O 2p character with non-negligible contributions from Ti 3d states, mainly in its lower part. It is less sensitive to GW-corrections, which almost rigidly shift the bands towards lower energies. As a consequence, the LDA and GW-bandwidths along the Δ line (4.15 eV and 4.11 eV, respectively) are both in very good agreement with the value of 4.2 eV measured in angle-resolved photoemission [6]. Similarly, the total $R_{1,v}$–$R_{12,v}$ bandwidth (see also figure 3) turns out to be 4.8 eV in the LDA and 4.9 eV with quasiparticle corrections.

A major difference between the LDA and GW-results regards the direct band gaps, which

roughly differ by about 3 eV. The onset for optical absorption was measured at 3.2 eV by Cardona [53] and at 3.34 eV by Blazey [54], and interpreted as a $\Gamma_{15,v} \rightarrow \Gamma_{25',c}$ transition. The strong absorption peaks at $\simeq$4–5 eV were attributed to vertical transitions at X and M, respectively. On the other hand, the fundamental gap derived from combined photoemission and inverse photoemission spectra, which is free from excitonic effects, was estimated to be (3.3 $\pm$ 0.5) eV [55]. With respect to these experimental values, the LDA $E_g(\Gamma)$ is underestimated by almost 1 eV, while the GW-value is overestimated by about 2 eV (see table 7). In this respect, the inclusion of self-energy corrections at a perturbative level does not improve the LDA. This issue is discussed in the next section, in relation to the validity of our model screening for transition metal oxides such as $SrTiO_3$.

Table 7. Computed E_g-values for direct transitions from the VB to the CB of cubic $SrTiO_3$, in eV. The minimal gap is also given.

$SrTiO_3$	$E_g(\Gamma)$	E_g(X)	E_g(M)	E_g(R)	Minimal gap
LDA [50]	2.16				1.79 (R–Γ)
LDA [58]	3.77	4.1		5.2	2.88 (R–Γ)
This work					
LDA	2.24	2.85	4.17	4.82	1.90 (R–Γ)
LDA + GW	5.42	6.10	7.29	8.15	5.07 (R–Γ)

7. Discussion

The agreement of our numerical results with the available experimental data is rather inhomogeneous: while for MgO and SrO a reasonable agreement is found, for $SrTiO_3$ the QP bands around the Fermi level seem to be worse than the LDA ones. It is the aim of this section to discuss our results with respect to two points: on the one hand, the quality of the ground-state calculation from which the perturbative GW-calculation starts; on the other hand, the reliability of our model dielectric function used in the calculation of the QP spectra of the oxides considered here.

We have found that the values of the direct gaps are very sensitive to the value of the lattice parameter. A good description of the ground-state structural properties is thus a prerequisite to obtaining QP spectra that can be compared to experimental data reliably. This is especially the case for MgO and SrO. In table 8 the relative variations $\Delta_g(\vec{k})$ of the direct gaps, both in the LDA and in the GW-approximation, are given as a function of the lattice parameter. One can note that:

(i) The largest variations of the direct gaps $\Delta_g(\vec{k})$ are nearly always obtained at the LDA level.
(ii) $\Delta_g(\vec{k})$ depends on the actual $\vec{k}$-point, consistently with the character of the wavefunction. The largest $\Delta_g(\vec{k})$ are generally found for the strongest bonding–antibonding combinations across the gap.
(iii) Increasing $\Delta_g(\Gamma)$ is found for $SrTiO_3$, SrO and MgO, in ascending order.

One should thus be careful when discussing the quality of the self-energy corrections to the electronic structure, since it may be strongly dependent on variables, such as the lattice parameter, which are *external* to the theory itself. Our data for MgO, obtained at the experimental lattice constants a_{exp}, compare well with other more sophisticated, *ab initio* GW-results also using a_{exp} [15, 39], as far as the direct gaps are concerned (see table 3). Both

Table 8. The dependence of the direct gaps $E_g(\vec{k})$ of MgO, SrO and $SrTiO_3$ at high-symmetry points $\vec{k}$ of the Brillouin zone as a function of the relative variations of the lattice parameter $(a_{th}-a_{exp})/a_{exp}$. The function Δ_g is defined as $\{[E_g(a_{th})-E_g(a_{exp})]/E_g(a_{exp})\}a_{exp}/(a_{th}-a_{exp})$. The values are computed either by using the LDA, or by including quasiparticle corrections within the GW-approximation.

	MgO	SrO	$SrTiO_3$
$(a_{th}-a_{exp})/a_{exp}(\%)$	−2.0	−1.7	−1.3
$\Delta_g^{LDA}(\Gamma)$	−6.4	−5.4	−1.7
$\Delta_g^{GW}(\Gamma)$	−4.1	−3.6	
$\Delta_g^{LDA}(X)$	−0.7	1.5	−2.2
$\Delta_g^{GW}(X)$	−0.7	0.6	
$\Delta_g^{LDA}(L)$	−2.7	−2.5	−4.4
$\Delta_g^{GW}(L)$	−2.1	−2.0	

for MgO and for SrO, a fair accordance with experimental data is found when adopting a_{exp}. We thus conclude that, still at the level of the ground-state structural properties, one should obtain a good agreement with experimental data (for example, by using generalized gradient corrections to the LDA) before starting the calculation of the quasiparticle energies.

Care must also be taken when comparing the theoretical gaps and those derived from optical measurements, because of the existence of excitonic effects in the latter, not accounted for in the present theory. For MgO, these effects should be rather small, as suggested experimentally by Roessler and Walker [42] and calculated by Benedict and co-workers [60]. For SrO and $SrTiO_3$ there is still a lack of the *ab initio* calculations of one- and two-particle excitations required to address this issue fully.

Another important point is the quality of the quasiparticle corrections, in relation to the model dielectric function $\epsilon(q,\tilde{\rho})$ used in the GW-calculation. As is evidenced by equation (6), the screening depends on the value of the optical dielectric constant ϵ_∞ of the oxide. As in the previous discussion regarding the lattice parameter, one can use either the experimental optical dielectric constant available in the literature, or compute it in the framework of the self-consistent theory adopted, such as the DFT. In a recent paper, Shirley [39] obtained for MgO a theoretical optical dielectric constant, at the *experimental* lattice parameter, $\epsilon_\infty^{(th)}=3.03$ in the LDA, to be compared with the measured $\epsilon_\infty=2.95$ [38]. Extrapolating our results—obtained with $\epsilon_\infty=2.95$ and $\epsilon_\infty=3.50$ (see section 4)—we can conclude that our quasiparticle energies would vary by less than 0.1 eV when passing from $\epsilon_\infty=2.95$ to $\epsilon_\infty^{(th)}=3.03$. However, a more satisfactory theoretical framework would be to compute ϵ_∞ from first principles, in conjunction with the use of an approximation for the exchange–correlation energy, capable of reproducing the experimental lattice constant. Although in the present case the results would not be much affected, this would open the way to the calculation of quasiparticle excitations of systems for which no experimental measurements of the optical dielectric constant are available. On the other hand, the use of model dielectric functions might open the possibility to treat complex systems consisting of many inequivalent atoms, such as low-symmetry crystals, surfaces and heterostructures.

Considering the numerical results obtained, and the previous discussion, we note that the model dielectric function works reasonably well for both MgO and SrO, which are compounds with fundamental gaps much larger than those of the semiconductors ZnSe, GaN and SiC previously studied with the same method [21, 23]. We thus conclude that the validity of the

screening model (equation (6)) is neither a function of the gap value nor a function of the ionocovalent character of the bonding in the crystal under study. On the other hand, it fails when applied to $SrTiO_3$, a transition metal oxide characterized by a moderate optical gap (slightly larger than 3 eV according to references [6, 54]).

In order to clarify the reasons for such a failure, we computed the bare exchange contribution to the QP gap at the Γ point, for both MgO (10.46 eV) and $SrTiO_3$ (12.28 eV), in first-order perturbation theory. This difference stems from the different character of the states at the bottom of the conduction bands, which have a Ti 3d character in the case of $SrTiO_3$, and are much flatter than those of MgO, having a dominant Mg 3s character. This is fully consistent with the stronger localization of the Ti 3d states, which could make our treatment of local field effects (see equations (6) and (7)) rather inappropriate. In fact, the choice of the effective density $\tilde{\rho}_{n\bar{k}}$ (equation (8)) takes into account the different localization of the states only through their superposition with the electron density $\rho(\vec{r})$. Moreover, its definition contains an ambiguity, since its precise value depends on the core–valence partitioning of $\rho(\vec{r})$. It is interesting to consider the extreme limit in which $\epsilon(q, \tilde{\rho})$ is no longer q-dependent and is simply replaced by the optical dielectric constant ϵ_∞. In this limit of screening, the only contribution to the GW-correction to the DFT-LDA gap comes from the screened exchange term, since the Coulomb hole gives a rigid shift equal for all the bands. Interestingly, this correction provides gap values equal to 4.3 eV for MgO and 2.7 eV for $SrTiO_3$, in much better agreement with experiments in the latter case than when using $\epsilon(q, \tilde{\rho}_{n\bar{k}})$ given by equation (6). This indicates the need for a better inclusion of local field effects in the model dielectric function for transition metal oxides, such as $SrTiO_3$. Another source of failure relating to $SrTiO_3$ could be also the use of a perturbative GW-scheme: a possible solution to this issue would be the use of an efficient self-consistent GW-approach which has been shown to give good results even for systems in which d orbitals play a fundamental role [61].

8. Conclusions

We have calculated the ground-state properties of the cubic oxides MgO, SrO and $SrTiO_3$ within the DFT-LDA, and applied a perturbative GW-method, based on a dielectric model which includes approximately local field and dynamical effects, to determine their quasiparticle energies. We have tested the dependence of the calculated spectra on the parameters entering the calculation, such as the optical dielectric constant ϵ_∞ and the lattice parameter a. In particular, we have shown that quasiparticle energies in alkaline-earth oxides are sensitive functions of the lattice parameter, even at the LDA level. As a consequence, the use of either the experimental or the theoretical values for a can influence the quality of the results whenever $a_{\rm th}$ differs from $a_{\rm exp}$.

Through a careful comparison with the available experimental data and previous *ab initio* GW-calculations, we have showed that the simplified GW-method works reasonably well for systems, such as MgO and SrO, in which the electronic states of the valence band and the bottom of the conduction band mainly consist of s- and p-like states. Moreover, in the three oxides, GW-corrections have been found to be crucial to account for the energies of semicore electron states, such as O 2s, Ti 3s, Ti 3p, Sr 4s and Sr 4p, which agree well with the peak positions recorded in photoemission spectra. When localized d-like states contribute to bands around the Fermi level, our method produces an overestimation of the self-energy corrections. This is the case for $SrTiO_3$, for which it is not clear at this stage whether a higher-order perturbative approach, in which the LDA wavefunctions are renormalized, is needed, or whether this failure calls for a more refined treatment of local field effects.

Acknowledgments

We thank Lucia Reining for fruitful discussions and a careful reading of the manuscript, Tristan Albaret for his help in generating the pseudopotentials and Eric Shirley for kindly providing us with unpublished results on self-energy corrections for MgO. Computing resources were granted by the IDRIS/CNRS computational centre in Orsay, under project 980864. GC acknowledges support from the Commission of the European Communities (framework IV) programme under the Networks scheme.

References

[1] Noguera C 1996 *Physics and Chemistry of Oxide Surfaces* (Cambridge: Cambridge University Press)
[2] Bechstedt F 1992 *Adv. Solid State Phys.* **32** 161
[3] Noguera C and Mackrodt W C 2000 *J. Phys.: Condens. Matter* **12** 2163
[4] Mackrodt W C, Harrison N M, Saunders V R, Allan N L and Towler M D 1996 *Chem. Phys. Lett.* **250** 66
[5] Tjeng L H, Vos A R and Sawatzky G A 1990 *Surf. Sci.* **235** 269
[6] Brookes N B, Law D S-L, Padmore T S, Waeburton D R and Thornton G 1988 *Solid State Commun.* **57** 473
[7] Raikar G N, Hardman P J, Muryn C A, van der Laan G, Wincott P L, Thornton G and Bullett D W 1991 *Solid State Commun.* **80** 423
[8] Hardman P J, Wincott P L, Thornton G, Bullett D W and Dale P A D M A 1994 *Phys. Rev.* B **49** 7170
[9] Hedin L 1965 *Phys. Rev.* **139** A796
Hedin L and Lundqvist S 1969 *Solid State Physics* vol 23 (New York: Academic) p 1
[10] Hybertsen M S and Louie S G 1986 *Phys. Rev.* B **34** 5390
[11] Godby R, Schlüter M and Sham L J 1988 *Phys. Rev.* B **37** 10 159
[12] Rohlfing M, Krüger P and Pollmann J 1998 *Phys. Rev.* B **57** 6485
[13] Shirley E L 1998 *Phys. Rev. Lett.* **80** 794
[14] Králik B, Chang E K and Louie S G 1998 *Phys. Rev.* B **57** 7027
[15] Schömberger U and Aryasetiawan F 1995 *Phys. Rev.* B **52** 8788
[16] Pulci O, Onida G, Del Sole R and Reining L 1998 *Phys. Rev. Lett.* **81** 5347
[17] Rohlfing M and Louie S G 1999 *Phys. Rev. Lett.* **83** 856
[18] Bechstedt F and Del Sole R 1988 *Phys. Rev.* B **38** 7710
[19] Gygi F and Baldereschi A 1989 *Phys. Rev. Lett.* **62** 2160
[20] Bechstedt F, Del Sole R, Cappellini G and Reining L 1992 *Solid State Commun.* **84** 765
[21] Palummo M, Del Sole R, Reining L, Bechstedt F and Cappellini G 1995 *Solid State Commun.* **95** 393
[22] Cappellini G, Fiorentini V, Tenelsen K and Bechstedt F 1996 *Mater. Res. Soc. Symp. Proc.* **395** 429
[23] Wenzien B, Cappellini G and Bechstedt F 1995 *Phys. Rev.* B **51** 14 701
[24] Wenzien B, Käckell P, Bechstedt F and Cappellini G 1995 *Phys. Rev.* B **52** 10 897
[25] Fulde P 1991 *Electron Correlations in Molecules and Solids* (Berlin: Springer)
[26] Kohn W and Sham L J 1965 *Phys. Rev.* **140** A1133
[27] Hybertsen M S and Louie S G 1988 *Phys. Rev.* B **37** 2733
[28] Reining L, Onida G and Godby R W 1997 *Phys. Rev.* B **56** 4301
[29] Levine Z H and Louie S G 1982 *Phys. Rev.* B **25** 6310
[30] Cappellini G, Del Sole R, Reining L and Bechstedt F 1993 *Phys. Rev.* B **47** 9892
[31] Ceperley D M and Alder B J 1980 *Phys. Rev. Lett.* **45** 566
[32] Gonze X, Stumpf R and Scheffler M 1991 *Phys. Rev.* B **44** 8503
[33] Troullier N and Martins J L 1991 *Phys. Rev.* B **43** 1993
[34] Monkhorst H J and Pack J D 1976 *Phys. Rev.* B **13** 5188
[35] Gygi F and Baldereschi A 1986 *Phys. Rev.* B **34** 4405
[36] Taurian O E, Springborg M and Christensen N E 1985 *Solid State Commun.* **55** 351
[37] Kowalczyk S P, McFeely F R, Ley L, Gritsyna V T and Shirley D A 1977 *Solid State Commun.* **23** 161
[38] Whited R C, Flaten C J and Walker W C 1973 *Solid State Commun.* **13** 1903
[39] Shirley E 1998 *Phys. Rev.* B **58** 9579
[40] Sangster M J L, Peckam G and Saunderson D H 1970 *J. Phys. C: Solid State Phys.* **3** 1026
[41] Chang K J and Cohen M L 1984 *Phys. Rev.* B **30** 4774
[42] Roessler D M and Walker W C 1967 *Phys. Rev.* **159** 733
[43] Pandey R, Jaffe J E and Kunz A B 1991 *Phys. Rev.* B **43** 9228

[44] van Doveren H and Verhoeven J A Th 1980 *J. Electron Spectrosc. Relat. Phenom.* **21** 265
[45] Rao A S and Kearney R J 1979 *Phys. Status Solidi* b **95** 243
[46] Kaneko Y and Koda T 1988 *J. Cryst. Growth* **86** 72
[47] Hasegawa A and Yanase A 1980 *J. Phys. C: Solid State Phys.* **13** 1995
[48] Zupan A, Petek I, Causà M and Dovesi R 1993 *Phys. Rev.* B **48** 799
[49] Cortona P and Villafiorita Monteleone A 1996 *J. Phys.: Condens. Matter* **8** 8983
[50] Kimura S, Yamauchi J, Tsukada M and Watanabe S 1995 *Phys. Rev.* B **51** 11 049
[51] King-Smith R D and Vanderbilt D 1994 *Phys. Rev.* B **49** 5828
[52] Dore P, Paolone A and Trippetti R 1996 *J. Appl. Phys.* **80** 5271
[53] Cardona M 1965 *Phys. Rev.* **140** A651
[54] Blazey K W 1971 *Phys. Rev. Lett.* **27** 146
[55] Tezuka Y, Shin S, Ishii T, Ejima T, Suzuki S and Sato S 1994 *J. Phys. Soc. Japan* **63** 347
[56] Weyrich K H and Siems R 1985 *Z. Phys.* B **61** 63
[57] Fischer G J, Wang Z and Karato S-I 1993 *Phys. Chem. Minerals* **20** 97
[58] Xu Y N and Ching W Y 1991 *Phys. Rev.* B **44** 7787
[59] Shirley E 1999 private communication
[60] Benedict L X, Shirley E L and Bohn R B 1998 *Phys. Rev. Lett.* **80** 4514
[61] Massidda S, Continenza A, Posternak M and Baldereschi A 1997 *Phys. Rev.* B **55** 13 494